On the Development of a Three-Dimensional Transient Thermal Model to Predict Ingot Cooling Behavior during the Start-Up Phase of the Direct Chill-Casting Process for an AA5182 Aluminum Alloy Ingot

J. SENGUPTA, S.L. COCKCROFT, D.M. MAIJER, M.A. WELLS, and A. LAROUCHE

The control of the heat transfer during the start-up phase of the direct-chill (DC) casting process for aluminum sheet ingots is critical from the standpoint of defect formation. Process control is difficult because of the various inter-related phenomena occurring during the cast start-up. First, the transport of heat to the mold is altered as the ingot base deforms and the sides are pulled inward during the start-up phase. Second, the range of temperatures and water flow conditions occurring on the ingot surface as it emerges from the mold results in the full range of boiling-water heat-transfer conditions—*e.g.*, film boiling, transition boiling, nucleate boiling, and convection—making the rate of transport highly variable. For example, points on the ingot surface below the point of water impingement can experience film boiling, resulting in the water being ejected from the surface, causing a dramatic decrease in heat transfer below the point of ejection. Finally, the water flowing down the ingot sides may enter the gap formed between the ingot base and the bottom block due to butt curl. This process alters the heat transfer from the base of the ingot and, in turn, affects the surface temperature on the ingot faces, due to the transport of heat within the ingot in the vertical direction. A comprehensive mathematical model has been developed to describe heat transfer during the start-up phase of the DC casting process. The model, based on the commercial finite-element package ABAQUS, includes primary cooling *via* the mold, secondary cooling *via* the chill water, and ingot-base cooling. The algorithm used to account for secondary cooling to the water includes boiling curves that are a function of ingot-surface temperature, water flow rate, impingement-point temperature, and position relative to the point of water impingement. In addition, a secondary cooling algorithm accounts for water ejection, which can occur at low water flow rates (low heat-extraction rates). The algorithm used to describe ingot-base cooling includes both the drop in contact heat transfer due to gap formation between the ingot base and bottom block (arising from butt curl) as well as the increase in heat transfer due to water incursion within the gap. The model has been validated against temperature measurements obtained from two 711 × 1680 mm AA5182 ingots, cast under different start-up conditions (nontypical "cold" practice and nontypical "hot" practice). Temperature measurements were taken at various locations on the ingot rolling and narrow faces, ingot base, and top surface of the bottom block. Ingot-base deflection data were also obtained for the two test conditions. Comparison of the model predictions with the data collected from the cast/embedded thermocouples indicates that the model accounts for the processes of water ejection and water incursion and is capable of describing the flow of heat in the early stages of the casting process satisfactorily.

I. INTRODUCTION

THE semicontinuous direct-chill (DC) casting process (Figure 1[1,2]) has been used almost exclusively to produce aluminum sheet ingots during the past 60 years, owing to its ability to produce high-quality ingots at a relatively low operating cost. At the start of the cast, a bottom or starter block is partially inserted into an open rectangular water-cooled mold, which is typically ~120 to 150 mm in height. The process starts with the introduction of superheated liquid metal to the mold. Once the molten metal fills the mold to a prescribed height, the bottom block is gradually lowered into a casting pit and the partially solidified ingot is withdrawn from the mold. The ingot is lowered at a predetermined casting speed, which initially varies with time and is tailored to suit the alloy. The process is semicontinuous, in that, once the ingot has reached the desired length (usually ~4 to 10 m), the casting is stopped and the flow of liquid metal is suspended.

During this process, the ingot is first cooled by the mold (primary cooling) and then cooled through direct contact with water as it emerges from the mold (secondary cooling). At steady state, which is usually achieved within a cast length of ~0.5 to 1 m,[3] approximately 80 pct of the total heat is removed by the secondary cooling and approximately 20 pct is removed by primary cooling. In the start-up phase, this breakdown is different, as a substantial amount of the heat is initially transferred to the bottom block.

J. SENGUPTA, formerly Graduate Student, Department of Metals and Materials Engineering, The University of British Columbia, is Research Associate and NSERC Canada Fellow, Department of Mechanical and Industrial Engineering, University of Illinois at Urbana–Champaign, Urbana, IL 61801. S.L. COCKCROFT, Associate Professor and Head, and D.M. MAIJER and M.A. WELLS, Assistant Professors, are with the Department of Metals and Materials Engineering, The University of British Columbia, Vancouver, BC, Canada V6T 1Z4. Contact e-mail: steve@cmpe.ubc.ca A. LAROUCHE, Principal Scientist, is with the Applied Research Group, Arvida Research and Development Centre, Alcan International Ltd., Jonquière, Canada G7S 4K8.

Manuscript submitted May 7, 2003.

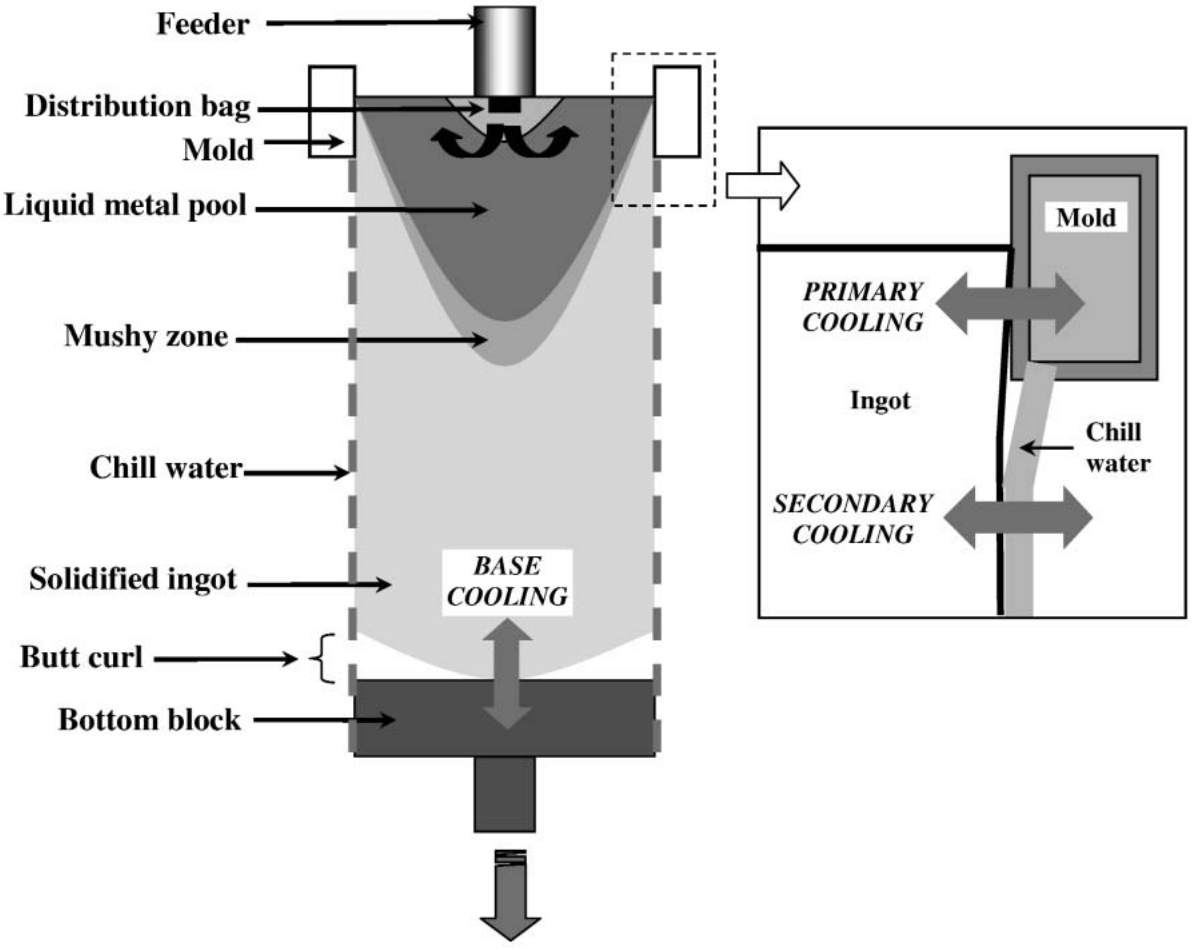

Fig. 1—Schematic of the DC casting process for aluminum sheet ingots and various cooling phenomena active during the process.[1,2]

From the standpoint of defect control, the start-up phase of the DC casting process is typically the most problematic. The quality issues of major concern include hot tearing, cold cracking, and dimensional control.[3] For example, wide-freezing-range alloys such as AA5182 tend to be prone to hot tears, which typically form during the start-up phase in close proximity to the ingot base and are usually found in roughly the center third of the rolling face.[4] Additionally, large thermal stresses can develop in the ingot base during start-up, causing upward deformation of the corners, referred to as butt curl,[1,2,3] as shown in Figure 1. The development of significant amounts of butt curl begins when the cooling water hits the ingot surface.[5] The rate of deformation of the ingot base has been observed to reach a maximum shortly after the water impingement on the surface of the ingot and then to decay to a very low value after a few minutes of the casting process.[6]

The trend in the industry has been to control the rate of heat transfer during the critical start-up phase by varying the bottom-block filling rate, casting speed, and water flow rates.[7] Additional strategies include the use of a variety of water-cooling systems, including Alcoa's CO_2 injection,[8] Wagstaff's Turbo process,[9] and Alcan's Pulse Water technique.[10] Attempts have also been made to develop an optimized bottom-block shape empirically.[11,12] These technologies, and the so-called "casting recipes" governing the start-up procedure, have evolved largely through trial and error and vary with the size of ingot and alloy type.

To date, relatively little fundamental work has been done to rationalize the design of the casting process with regard to controlling the final ingot quality. The development of numerous three-dimensional (3-D) computer models to describe the heat transfer and evolution of stress and strain in DC cast ingots has begun to have an impact on the evolution in the design and operation of the process. However, improvements are needed to capture the various inter-related heat-transfer phenomena occurring during the process, particularly during the start-up regime.

II. BACKGROUND AND LITERATURE REVIEW

Since the early 1990s, a number of researchers have developed mathematical models to describe heat transfer during the transient start-up phase of the DC casting process. Fjær and Mo[13] and Schneider and Jensen[14] were among the first to develop two-dimensional (2-D) axisymmetric thermal models to calculate the temperature profile in DC-cast billets in order to compute the thermal stresses. Fjær and Mo accounted for the development of the air gap between the

billet and the bottom block (associated with butt curl) by reducing the heat-transfer coefficient applied to the ingot base from 2000 to 300 W m^{-2} K^{-1} with time. A subsequent 3-D finite-element version of this model for ingot casting[15,16] included the effect of water incursion. The authors found that butt-curl evolution is highly sensitive to the degree of secondary cooling and heat transfer to the bottom block.

Hannart *et al.*[17] developed a coupled 3-D thermomechanical model of ingot casting based on the finite-element (FE) method. Their model used temperature- and water flow rate–dependent heat-transfer correlations to describe secondary cooling and a displacement-dependent boundary condition applied to the base of the ingot to account for the influence of butt curl on heat transfer. The effect of water incursion was ignored, and the bottom block was treated as a surface with a constant temperature of 100 °C. Drezet and Rappaz[18] also developed a coupled 3-D thermomechanical model. In their model, the bottom block was treated as a surface at a constant temperature. For secondary cooling, they adopted a positionally dependent surface heat flux based on an inverse analysis of thermocouple data obtained during steady-state operation. The heat-transfer coefficient at the ingot base was reduced from 2000 to 200 W m^{-2} K^{-1} to account for ingot-base deflection. The effect of water incursion was ignored in the analysis.

Wiskel and Cockcroft[19,20] described experiments conducted on DC cast AA5182 sheet ingots and an inverse heat-conduction analysis of the experimental results. They concluded that water incursion has a strong effect on ingot-base cooling and also suggested a link between the ingot surface temperature at the point of water impingement and the subsequent rate of heat extraction in the secondary cooling regime.

Du *et al.*[21] included the bottom block in a coupled 3-D thermomechanical analysis. They employed a temperature- and water flow rate–dependent relationship to quantify secondary-cooling heat transfer based on temperature measurements obtained during steady-state operation. A function relating the heat-transfer coefficient to the interfacial gap opening was used in the analysis. The model predictions were compared with experimentally measured data obtained using thermocouples embedded in the ingot base.

Fjær *et al.*[22] investigated the start-up heat-transfer conditions using a transient 3-D simulation, which coupled thermal, stress, and fluid-flow phenomena. The boundary condition applied at the ingot base/bottom-block interface accounted for air-gap formation and included the effects of conduction and radiation. The heat-transfer coefficient was assumed to depend on the surface temperature of the ingot base and normal pressure fields computed by the stress analysis. The effect of water incursion was also included in the analysis. Those areas of the base in contact with water adopted a high heat-transfer coefficient in the range of 2000 to 3500 W m^{-2} K^{-1}. A provision was added that reduced the heat-transfer coefficient to 200 W m^{-2} K^{-1} for the ejection of water from the ingot base at high temperatures due to film boiling. The model predictions at the base of the ingot and inside the bottom block were compared to measured values and were found to be in good agreement. The authors experienced two difficulties while validating their thermal model: (1) most of the thermocouples near the ingot base failed during the evolution of butt curl, and (2) fine-tuning the heat-transfer coefficients for ingot-base cooling was not possible due to the long computing times. The authors also indicated that the water-incursion criteria are closely related to the level of film boiling, which is also an important parameter for the development of butt curl.

Droste *et al.*[23] recently developed a coupled 3-D thermomechanical model, which employed a secondary cooling heat flux dependent on water flow rate and surface temperature. The authors included the effect of water incursion along the ingot base.

Sengupta *et al.*[24,25] included the bottom-block geometry in a 3-D sequentially coupled thermomechanical analysis for AA5182 sheet ingots and included the competing effects of the butt curl and water incursion to represent the base cooling. They showed that the bottom block plays a significant role in the heat transfer from the base of the ingot during start-up. In another article, Sengupta *et al.*[26] developed a 2-D model to examine the effect of water incursion and water ejection on the heat transfer during the start-up phase of AA5182 ingots. The model predictions were shown to agree well with thermocouple measurements taken in the vicinity of the rolling face of the ingot.

Based on the literature review focusing on modeling, it is clear that specific heat-transfer phenomena must be included to accurately describe heat transfer during the start-up phase of the DC casting process. With respect to secondary cooling, the phenomena include (1) surface-temperature dependence, (2) water-flow-rate dependence, (3) position dependence (relative to the point of water impingement) and (4) water ejection. With respect to heat transfer from the ingot base, the phenomena include (1) interaction with the bottom block, (2) ingot base/bottom block–gap dependence, and (3) dependence on water incursion.

This article describes the development of a comprehensive 3-D thermal model intended to capture most of the heat-transfer phenomena occurring during the start-up phase for a commercial DC ingot casting process. The model has been compared with industrial data collected from two AA5182 ingots: the first, cast under nontypical "hot" conditions and the second cast under nontypical "cold" conditions. The model has been developed using the commercial ABAQUS* FE package as part of a program to develop a 3-D coupled thermal/stress model to describe the thermomechanical behavior of the ingot during the start-up phase.

*ABAQUS is a trademark of ABAQUS Inc., Pawtucket, RI.

III. MODEL DEVELOPMENT

A significant part of the challenge in developing a fundamentally based approach to optimizing the start-up phase is that the ingot is simultaneously cooled by the mold (primary cooling), the chill water (secondary cooling), and the bottom block (base cooling). These three heat-transfer paths, shown schematically in Figure 1, are complex and inter-related.

A. *General Thermal Model Formulation*

Due to the time-dependent nature of the casting process, the heat-transfer model of the DC casting process must be transient. Owing to the range of temperatures experienced in the process, the model must account for any appreciable

temperature dependencies in thermophysical properties of the materials employed in the casting process. Fluid flow in the liquid due to filling of the mold has been ignored, and heat is assumed to be transferred by diffusion only. The governing partial differential equation describing the flow of heat is presented in Eq. [1]:

$$\rho\, c_p(T)\frac{\partial T}{\partial t} = \nabla(k(T)\nabla T) + \dot{Q} \qquad [1]$$

where ρ is the density in kg m^{-3}, c_p is the specific heat in J kg^{-1} K^{-1}, T is the temperature in K, k is the thermal conductivity in W m^{-1} K^{-1}, and $\dot{Q}$ is a volumetric source term associated with the latent heat of solidification in W m^{-3}.

B. *Calculation Domain and Geometry*

The calculation domain for the 3-D thermal analysis necessarily includes the ingot and bottom block. Taking advantage of the symmetry in heat transfer perpendicular to the rolling and narrow faces, the calculation domain employed in the 3-D analysis was reduced to quarter sections of the ingot and the bottom block. The FE mesh for the 3-D model, presented in Figure 2, consisted of eight-noded isoparametric brick elements, each with eight gauss integration points. The elemental size used for generating the FE mesh for the ingot and bottom block ranged from a minimum of ~4 mm to maximum of ~12.5 mm in side length. A higher mesh density along the vertical z direction was used to ensure proper accounting of the heat transfer within the impingement zone of the secondary cooling regime (a more detailed discussion is provided in Section III–E). A sensitivity analysis conducted with a 2-D section of the 3-D domain revealed that the model-predicted temperatures were not sensitive to mesh for the mesh resolution employed in the study.

The ingot mesh for the model was developed such that it consisted of horizontal layers of elements. Using this methodology, the gradual evolution of the metal level in the mold, as well as the ingot withdrawal from the mold, could be simulated. The timing for the addition of each layer was determined based on the mold filling times and casting speeds applied in the casting recipe. Typical industrial casting recipes have the bottom-block fill rate, metal-level height, bottom-block withdrawal rate (casting speed), and secondary cooling-water flow rate vary during start-up.

The mesh within the bottom block was generated with coincident nodes at the contact region between the ingot base and the bottom-block top surface. This allowed the exchange of heat across the interface to be captured within the model.

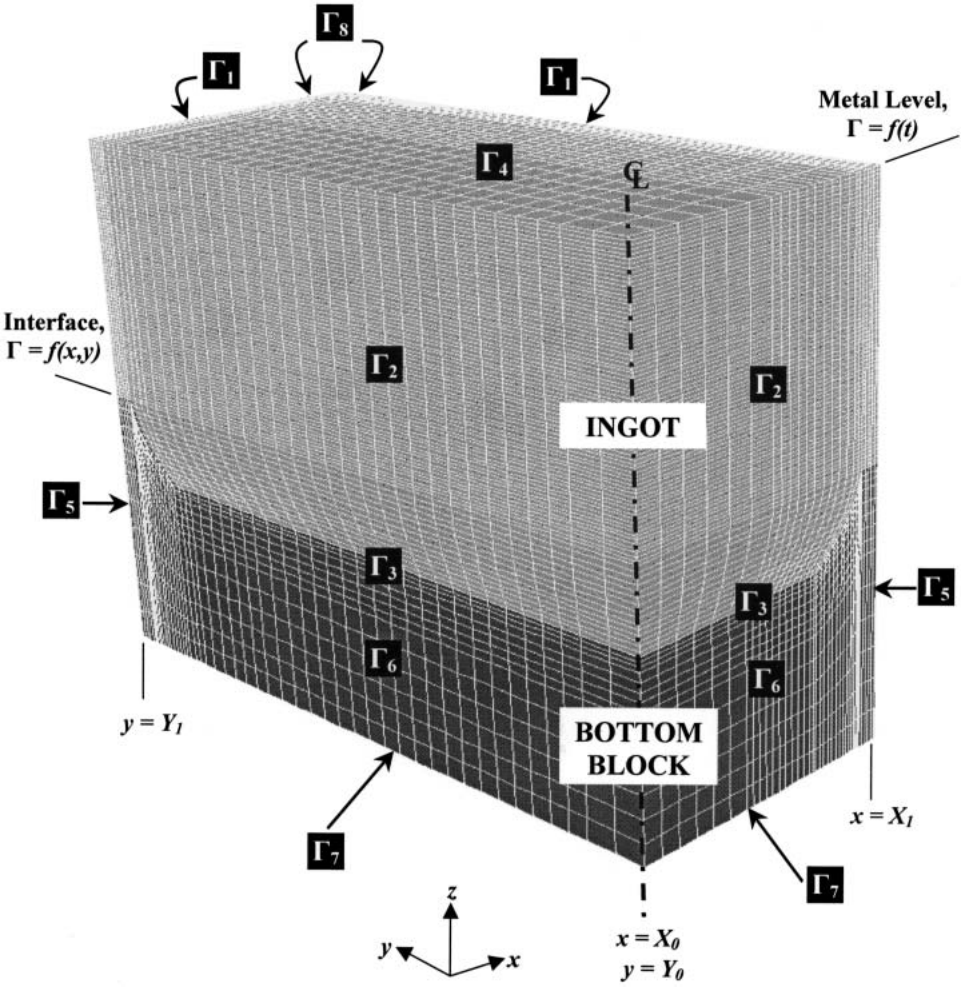

Fig. 2—The 3-D FE mesh for the ingot and bottom block. The various faces in the domain, on which thermal boundary conditions were applied, have also been indicated.

C. *Thermal Boundary Conditions*

1. *Ingot*

Referring to Figure 2, the external rolling and narrow faces of the ingot (surface Γ_1) extending above the bottom-block lip were treated using a Cauchy-type boundary condition according to Eq. [2]:

$$-k\left.\frac{\partial T}{\partial n}\right|_{x=X_1,y=Y_1} = h(T_{surf} - T_{sink}) \qquad [2]$$

where k is the thermal conductivity (W m^{-1} K^{-1}), $\partial/\partial n$ is the outward pointing derivative normal to the ingot surface, h is the effective heat-transfer coefficient (W m^{-2} K^{-1}), T_{surf} is the ingot surface temperature, T_{sink} is the far-field or sink temperature, X_1 is half the thickness of the ingot (equal to 355.5 mm), and Y_1 is half the width of the ingot (equal to 819 mm). The process for evaluating the appropriate heat-transfer coefficient (h) is described in detail in the subsequent section on implementation.

Owing to symmetry, the interior vertical faces (surface Γ_2) were assumed to be adiabatic according to Eq. [3]:

$$-k\left.\frac{\partial T}{\partial n}\right|_{x=X_0,y=Y_0} = 0 \qquad [3]$$

The base of the ingot in contact with the bottom block (interface Γ_3) was treated with a combination of a Cauchy-type boundary condition to describe interface-gap conductance and a Cauchy-type boundary condition to describe heat transfer to water, present due to the process of water incursion described earlier. The expression employed in the model is given in Eq. [4]:

$$-k\left.\frac{\partial T}{\partial n}\right|_{\Gamma=f(x,y)} = f_{wet}\, h_{water}\,(T_{ingot} - T_{water}) + h_{gap}\,(T_{ingot} - T_{bottomblock}) \qquad [4]$$

where h_{water} represents the heat-transfer coefficient to any water that may or may not be present (W m^{-2} K^{-1}), and h_{gap} represents the gap conductance at the interface (W m^{-2} K^{-1}). The variable $T_{bottomblock}$ appearing in the second term on the right-hand side of Eq. [4] represents the temperature in the bottom block directly adjacent to the point on the ingot base being processed. The term f_{wet} represents a factor used to account for the degree to which the ingot-bottom surface is wetted by the incursion water.

The top of the ingot (surface Γ_4) was assumed to be adiabatic according to Eq. [5]:

$$-k\left.\frac{\partial T}{\partial n}\right|_{\Gamma=f(t)} = 0 \qquad [5]$$

2. *Bottom block*

Referring to Figure 2, the external rolling and narrow faces of the bottom block (surface Γ_5) were treated with a Cauchy-type condition of the form shown in Eq. [2], with the term T_{surf} now set equal to the bottom-block temperature. The interior vertical faces (surface Γ_6) were assumed to be adiabatic due to symmetry and were treated with an expression of the form shown in Eq. [3]. Heat transfer from the top face of the bottom block (interface Γ_3), which is in contact with the ingot, was accounted for using an expression similar to that appearing in Eq. [4]. However, in the first term on the right-hand side, the variable T_{ingot} is replaced with $T_{bottomblock}$, and, in the second term on the right-hand side, the variables T_{ingot} and $T_{bottomblock}$ have been interchanged—*i.e.*, to reflect that the ingot is now the far-field or sink temperature. Heat transfer from the bottom face of the bottom block (surface Γ_7) was treated with an expression of the form shown in Eq. [2].

D. *Initial Conditions*

The nodes contained in the various layers of elements that are added sequentially to the solution domain are set at an initial temperature of 660 °C. The nodes contained within the bottom block were assigned an initial temperature of 25 °C.

E. *Implementation*

For the vertical rolling and narrow faces of the ingot (surface Γ_1), the magnitude of the heat-transfer coefficient appearing in Eq. [2] was varied to describe the various heat-transfer regimes shown schematically in Figure 3. The calculation was implemented within ABAQUS using the sfilm.f* subroutine. Four regions of heat transfer were defined based on their position relative to the top of the thermal-analysis domain and are described as follows.

*The sfilm.f user subroutine, provided by ABAQUS, can be accessed by a user to implement nonlinear Cauchy-type heat-transfer coefficients on different surfaces within the FE model.

1. *Primary or mold cooling*

Despite representing less than 20 pct of the total heat extracted from the solidifying ingot[1] during steady state, the heat transfer in the mold is critical, as it determines the surface temperature of the ingot at the point of exit from the mold, which, subsequently, influences the mode of boiling-water heat transfer—*e.g.*, film/nucleate boiling.[27] Moreover, it also has a significant impact on the ingot's surface quality.[28]

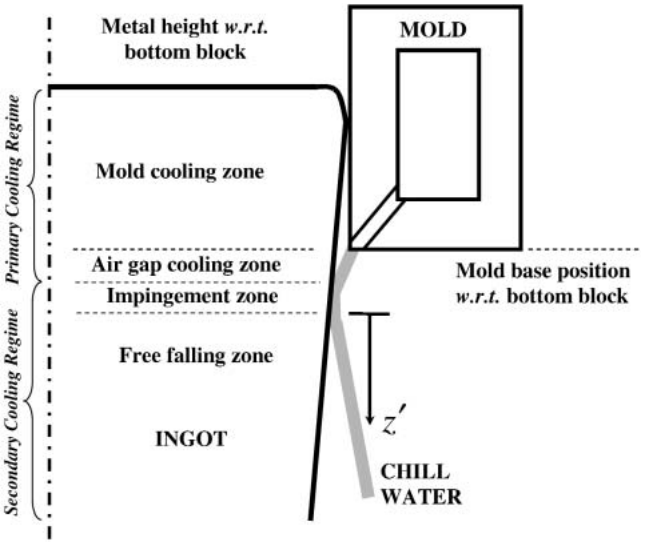

Fig. 3—Primary and secondary cooling regimes on the vertical face of the ingot.

Ho and Pehlke[29] and Nishida *et al.*[30] did fundamental work on the mechanisms of mold cooling in casting processes and found that, typically, high rates of heat transfer are observed in the early stages of a casting process when good physical metal/mold contact exists and that comparatively low heat transfer is seen in the later stages, as a gap forms due to volumetric shrinkage of the metal. The peak heat-transfer coefficient reported for aluminum contacting a chilled mold ranges from 2000 to 4000 W m^{-2} K^{-1}. By comparison, where a gap is present, the heat-transfer coefficient may be as low as approximately 150 W m^{-2} K^{-1}.[29]

The primary cooling experienced in the mold during DC casting is further complicated by the upward deformation of the ingot base (butt curl). This process tends to draw the sides of the ingot inward, altering the length of the gap (refer to Figure 3) which, in turn, changes the heat-transfer profile within the mold and, ultimately, the total heat removed by the mold.[31,32]

Referring to Figure 3, the heat transfer associated with the primary cooling to the mold has been characterized according to Eq. [6], which is applied over a region extending from the top of the ingot (meniscus) to the base of the mold. In this relationship, the heat-transfer coefficient is assumed to vary with the fraction solidified (temperature):

$$h = h_{\text{contact}} \cdot (1 - f_s) + h_{\text{gap}} \cdot f_s \qquad [6]$$

where h_{contact} was in the range of 1000 to 2000 W m^{-2} K^{-1} and was intended to reflect good thermal contact, h_{gap} was in the range of 50 to 200 W m^{-2} K^{-1} to reflect poor thermal contact associated with the gap formed inside the mold, and f_s is the volume fraction of solid, which was assumed to vary linearly between the liquidus (T_L) and solidus (T_S) temperatures for the AA5182 aluminum alloy.

2. *Air cooling*

Referring to Figure 3, this was applied to the regions of the calculation domain located below the base of the mold and above the water-impingement zone, at time t. In this regime, the heat-transfer coefficient was assumed to be in the range of $h = 50$ to 200 W m^{-2} K^{-1}.

3. *Secondary cooling*

On the sides of the ingot in contact with the secondary cooling water, there is the potential for up to four types of behavior, including (1) film boiling at high temperatures (>350 °C), (2) transition boiling between 200 °C and 350 °C, (3) nucleate boiling between 100 °C and 200 °C, and (4) convective cooling at temperatures lower than 100 °C.

Over the last few years, several studies[33–42] have conducted experimental quench tests in which samples were cooled by a water film to determine boiling curves by inverse heat-transfer analysis. Others[19,43–46] have used thermocouples embedded in ingots during casting combined with inverse heat-transfer analysis to determine the rate of transport. Weckman and Niessen[47] developed empirical relationships to describe the heat transfer. Grandfield *et al.*[48] described other relationships available in the literature. Recently, Sørheim *et al.*[49] have suggested a new method for inverse heat-transfer analysis for a 3-D problem. Combining the results from all of these studies, the following observations can be made.

1. The Leidenfrost temperature is sensitive to water flow rate and is observed to increase with increasing water flow rate.
2. The heat flux is low in the region of backflow above the impingement point and increases rapidly to a maximum value corresponding to the position where the water jet has maximum momentum. It then decreases with distance below the point of impingement as the water film loses momentum and the water temperature increases.[36]
3. The rate of heat extraction is also a strong function of ingot temperature at the point of water impingement. The dependence on impingement-point temperature is reported to be related to the capacity of the ingot to supply heat.[41]
4. The critical heat flux (peak) has been found to vary between 1.0 and 5.0 MW m^{-2}.[19,33,41,43,45,47,50] However, the critical heat-transfer coefficient has been found to vary between 40.0 and 50.0 kW m^{-2} K^{-1}.[33,35,37,42,46]
5. During the start-up phase, it is typical to have stable film boiling develop at certain locations on the ingot surface, which can result in water being ejected from the surface—refer to Figure 4.[36,51] Note: the formation of a stable vapor layer on the ingot surface does not necessarily result in, or form, due to the break-up of the water film into droplets, as illustrated in this schematic drawing. A stable film layer on the ingot surface can co-exist with a continuous film of water that has been ejected from the ingot surface.

In order to accurately capture heat-transfer phenomena occurring during the start-up phase, all of the previously cited phenomena related to secondary cooling must be included in the model.

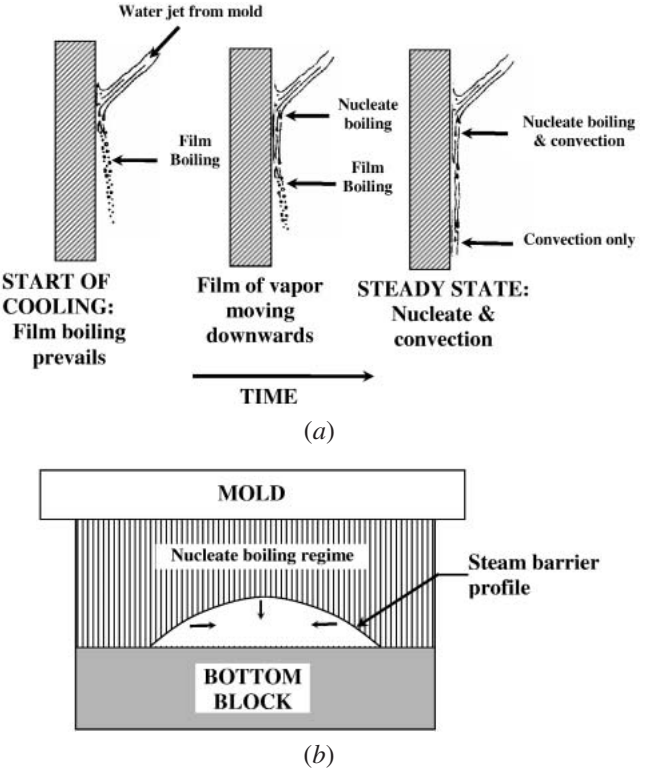

Fig. 4—(*a*) Phenomenon of water ejection or film boiling observed on the ingot surface during cast start-up,[36] and (*b*) evolution of parabola-shaped steam barrier in response to ingot surface temperature during a film boiling driven start-up phase.[51] The steam barrier collapses toward the center of the ingot surface as the casting process proceeds with time.

Referring to Figure 3, two distinct zones can be identified within the secondary cooling regime: (1) the water impingement zone (usually 10 to 15 mm in length, depending on the diameter of water holes at the base of the mold and angle of impingement) and (2) the free-falling or streaming zone.

A heat-transfer coefficient that is a function of the ingot-surface temperature, ingot-surface temperature at the water-impingement point, water flow rate (Q), and vertical distance below the impingement point (z') was adopted for the vertical faces of the ingot. Example boiling curves are presented in Figure 5(a) for a low water flow rate at $z' = 0$ mm and for a high water flow rate at $z' = 0$ and 50 mm, for the case where the impingement-point temperature is 575 °C. The effect of impingement-point temperature on the boiling curve is illustrated in Figure 5(b), which shows boiling curves for impingement-point temperatures of 575 °C and 485 °C (Q and z' held constant). During transient behavior in the start-up regime, the ingot-surface temperature at the impingement point varies with time, and, hence, each point on the surface of the casting was assigned its own unique boiling curve dependent on the impingement-point temperature experienced by that point on the ingot surface. The curves appearing in Figures 5(a) and (b) are based on a combination of experimental data obtained from previous studies conducted at the University of British Columbia[19,41] and Alcan.[36] The experimental data have been idealized by subdividing the data into a series of four different regimes in which the heat-transfer coefficient is assumed to vary linearly with temperature. The regimes, as labeled in Figure 5(a), are convection cooling (points A to B), nucleate boiling (points B to C), transition boiling (points C to D), and film boiling (points D to E). Point D has been taken as the Leidenfrost temperature. These correlations were implemented within the user-programmable subroutine sfilm.f in ABAQUS.

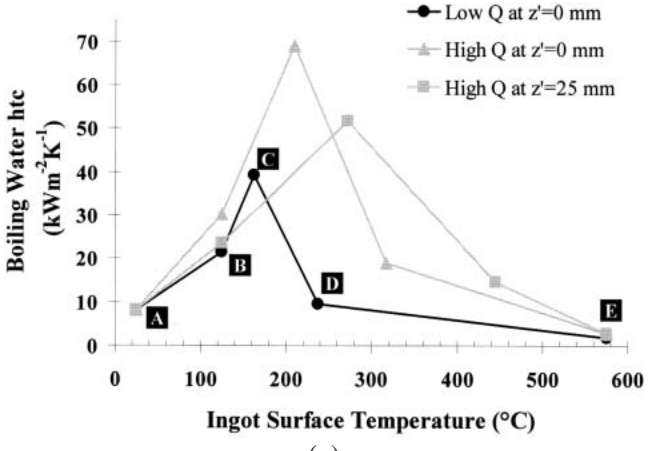

(*a*)

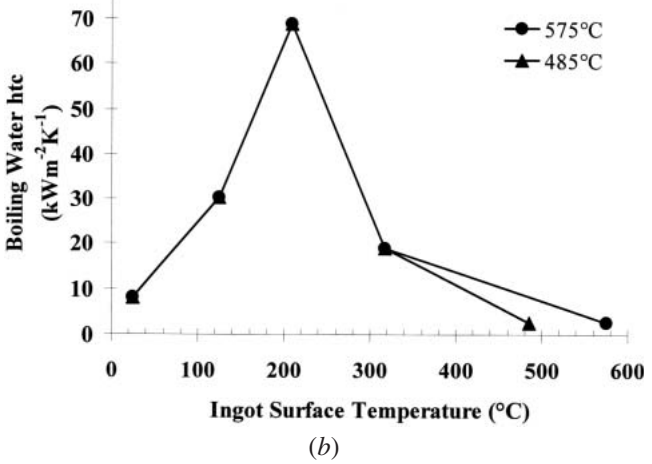

(*b*)

Fig. 5—(*a*) Boiling curves for different values of Q and z', which have been used to describe the secondary cooling process in the model; and (*b*) boiling curves for impingement point temperatures of 575 °C and 485 °C with Q and z' held constant.

In addition to the boiling-water correlations described earlier, a provision was also added to sfilm.f to simulate the effect of the water film being ejected from the ingot's vertical faces due to film boiling for the domain just below the impingement zone (commonly referred to as the free-falling zone, as shown in Figure 3). To facilitate this, the vertical ingot surfaces were divided into columns and rows of material-integration points. Using this scheme, any material-integration point on the surface Γ_1 could be referenced by the array $[i,j]$ (refer to Figure 6).

The algorithm used in the model to simulate the ejection of water tests the temperature at every stream position to see if it exceeds the Leidenfrost temperature at the beginning of every time increment (*i.e.*, the temperature on the boiling-water cooling curve above which the film-boiling process is predominant). If true, all the stream positions below it are assigned a heat-transfer coefficient of approximately 200 W m^{-2} K^{-1}, to simulate reduced heat transfer associated with water ejection. All the stream positions above the point of ejection are cooled as per the boiling curves described previously.

For the vertical exterior face of the bottom block (surface Γ_5 in Figure 2), the heat-transfer coefficient applied in Eq. [2] is identical to that used for the ingot vertical face subject to secondary cooling (water).

4. *Heat transfer by base cooling*

At the beginning of the casting process, when the liquid metal enters the bottom block, the rate of heat transfer from the molten metal to the cold bottom block will be high. After a short time, a small gap at the interface forms due to solidification, and the rate of heat transfer will drop. This gap will remain relatively small until the ingot sides come into contact with secondary water. At this point, the ingot base begins to deform upward macroscopically (peak displacements can reach a few tens of millimeters at the four corners) in response to the rapid thermal contraction of the sides.

This process, known industrially as butt curl, influences the development of the gap at the ingot base and, consequently, the rate of interface heat transport.[17,21,22] If the gap becomes large enough—refer to Figure 7—water falling down the side may enter the gap and enhance the heat transfer from the ingot base.[23] Hence, depending on the process conditions and location, the development of the gap can initially reduce heat transport from the base and then, later, increase it if entrained water comes into contact with the base.

The ingot/bottom-block interface (refer to Γ_3 in Figure 2) algorithm was implemented within ABAQUS using the user-defined subroutine gapcon.f.* In this algorithm, both the

*The gapcon.f user subroutine, provided by ABAQUS, can be accessed by a user to implement nonlinear heat-transfer coefficients active between two surfaces, which are in thermal contact with each other.

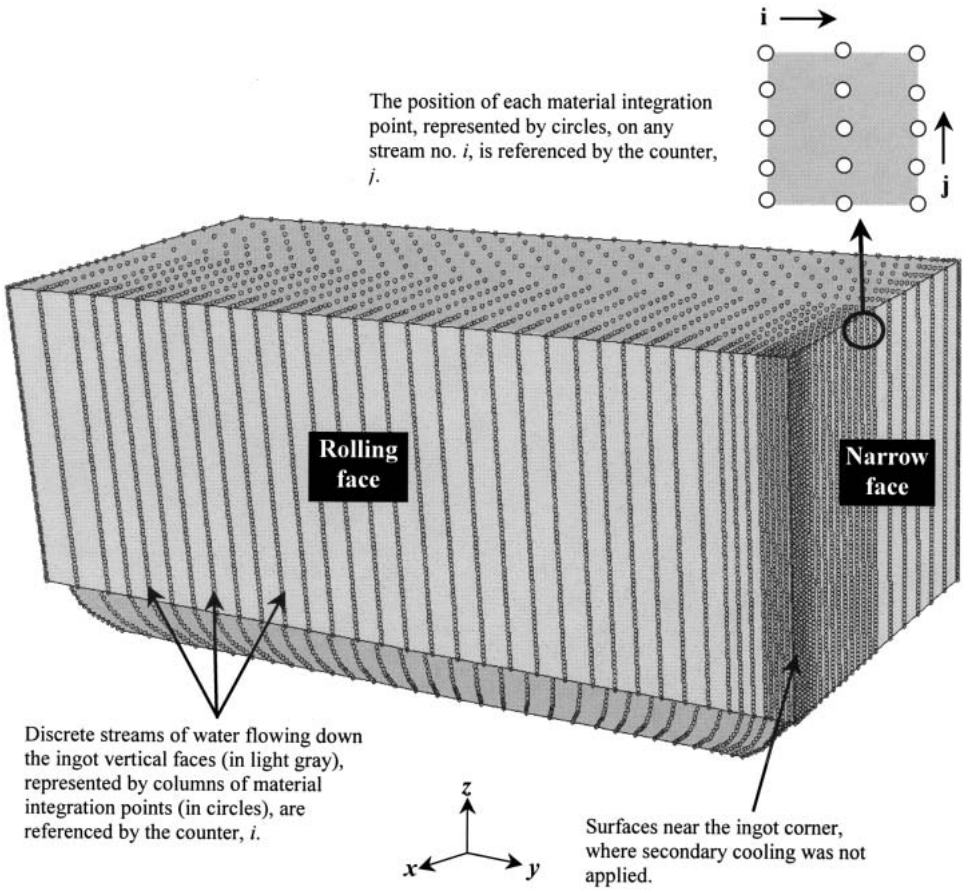

Fig. 6—Schematic representation of discrete water streams flowing down the ingot vertical surfaces (in light gray) in the 3-D FE thermal model, the formulation of which was required to implement the process of water ejection in the free falling zone. The surfaces near the corner are not included in the formulation.

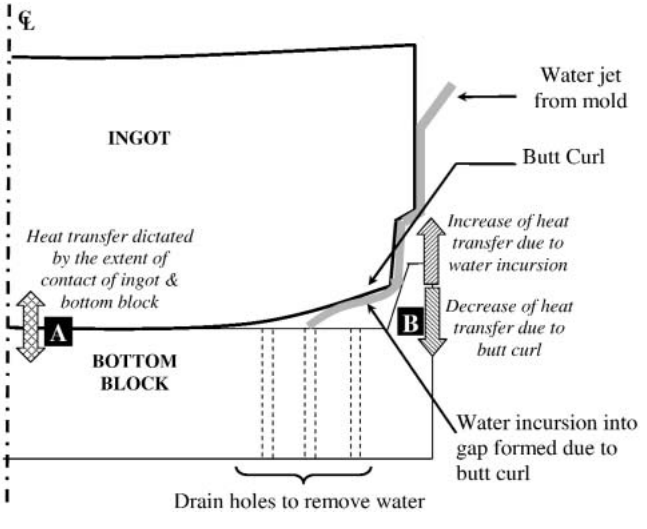

Fig. 7—The details of the ingot base cooling conditions during the start-up phase, showing the various heat-transfer processes occurring near the center of the ingot (region A) and the outer edges (region B).

gap-conductance term (h_{gap}) and water heat-transfer coefficient term (h_{water}) in Eq. [4] were ramped linearly with vertical displacement (butt curl). The h_{gap} value was ramped from 750 to 50 W m^{-2} K^{-1}, and h_{water} was ramped from 0 to a value corresponding to the boiling curve applicable at the local temperature (Q as per cast practice, $z' = 70$ mm, impingement temperature = 600 °C). In this manner, the loss in contact heat transfer due to increasing gap formation (butt curl) was offset by the increase in heat transfer due to water incursion. The gap-conductance term, is applied over the entire boundary Γ_3 during the analysis. In contrast, the term to account for water incursion, h_{water}, was applied to only a portion of the interface for both the ingot and bottom block—refer to the dark-gray and light-gray shaded regions in Figures 8(a) and (b), respectively. This feature was needed to address the fact that the water is generally removed from the gap by the drain holes located in the bottom block; thus, a significant portion of the center of the ingot base and bottom-block top face do not come into contact with the entrained water. Finally, an additional term, f_{wet}, was needed, as (1) not all of the water would necessarily become entrained in the gap, and (2) the degree to which the ingot-bottom face and bottom-block top face would be wetted would be different.

The vertical displacement of the base of the ingot was assumed to obey a parabolic relationship with distance and to also vary with time. The largest displacement was assumed to occur at the edges of the ingot, and no displacement was assumed to occur at the center. The variation in displacement with time was determined by fitting a simple polynomial to base-displacement measurements taken during casting—refer to Section IV.

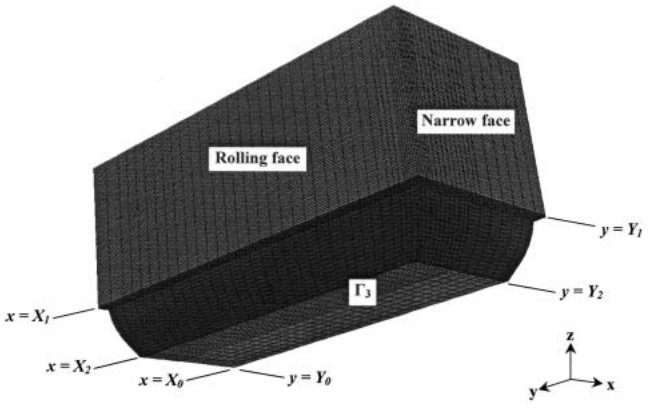

(*a*)

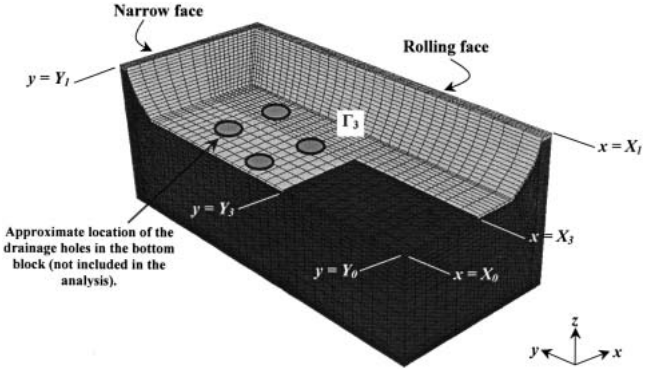

(*b*)

Fig. 8—Regions on the ingot–bottom block interface, Γ_3, which were assumed to be in contact with water entering the air gap during the process of incursion—for (*a*) ingot (in dark gray) and (*b*) bottom block (in light gray).

Table I. Thermophysical Properties of AA5182[2]

Variable	Temperature Range	Equation (T in °C)
Solidus (°C)	—	536
Liquidus (°C)	—	637
Conductivity	$T < 577$	$119.2 + 0.0623\ T$
(W m^{-1} K^{-1})	$536 \le T \le 637$	$594 - 0.484\ T - 0.00048\ T^2$
	$T > 637$	$69 + 0.033\ T$
Specific Heat	$T < 577$	$897 + 0.452\ T$
(J kg^{-1} K^{-1})	$536 \le T \le 637$	$-994.8 + 8\ T - 0.0074\ T^2$
	$T > 637$	1097
Density (kg m^{-3})	—	2400
Latent Heat	$536 \le T \le 637$	397,100
(J kg^{-1})		

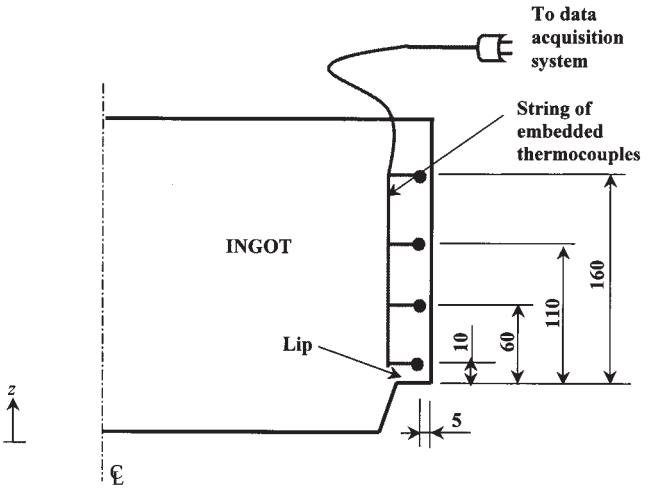

Fig. 9—Schematic of the arrangement of thermocouples instrumented adjacent to the ingot rolling and narrow faces. Note: Units are in millimeters.

Finally, for the bottom face of the bottom block (surface Γ_7), the heat-transfer coefficient appearing in Eq. [2] was set equal to 25 W m^{-2} K^{-1} to reflect natural convection to air.

F. *Materials Properties*

The thermophysical properties, solidus and liquidus temperatures, and the latent heat of solidification used in the analysis are temperature dependent and are presented in Table I after reference.[2] The density has been held constant at 2400 kg m^{-3}, to avoid altering the mass (since the volume of the computational domain does not vary with temperature). Since the model does not include any fluid-flow computations, the conductivity values above the liquidus are increased (~4 times) to approximate the effect of liquid convection in the sump.[18]

IV. INDUSTRIAL MEASUREMENTS

To obtain data suitable for verification of the model, industrial trials were performed at Alcan on a 711 × 1680 mm ingot of the AA5182 aluminum alloy. The bottom-block filling rate and water flow rate were varied to produce a nontypical cold start and a nontypical hot start. In the hot start, the bottom-block filling time was reduced by ~20 seconds and the water flow rate was reduced by ~25 pct relative to the cold start. The casting velocity was the same for the two start-up conditions. The cold casting was intended to produce an ingot that experiences little or no water ejection from the vertical surface, a large base deformation, and a substantial amount of water incursion during start-up. The hot casting was intended to produce an ingot that experiences film boiling and water ejection on the surface, a comparatively small amount of base deformation, and little or no water incursion.

To obtain temperature data, thermocouples were embedded at various locations in the ingot and in the bottom block. Three thermocouples were placed in the ingot adjacent to the rolling and narrow faces at heights of 10, 60, and 160 mm above the ingot lip, at a distance 5 mm below the surface, as shown in Figure 9. Two sets of thermocouples were used to record temperatures at the ingot base and the top surface of the bottom block. The thermocouples in the ingot base were frozen along the base of the solidifying ingot, and those in the bottom block were embedded along the top face of the bottom block. All the thermocouples were placed at a distance of 5 mm from the ingot/bottom-block surface. The positions (locations 2 through 8) of these thermocouple sets along the cross section are schematically presented in Figure 10. Location 4, near the center of the cross section, was not accessible in the case of the ingot due to the position of the distribution bag and metal feeder. As a result, temperature data for this location at the base of the ingot were not recorded. Temperatures were

recorded for the ingot and bottom block at locations 1, 9, and 10 near the ingot lip, as shown in Figures 10 and 11.

The thermocouples employed in the trials were a type-K (Nickel/Chrome-Nickel) with a diameter of 1/16 in. The thermocouples were protected from oxidation and/or corrosion by an Inconel sheath. A computer-based data-acquisition system was employed to record the thermocouple data at a frequency of 1 Hz.

The ingot-base deflection at two of the corners (diagonally opposite one another) was also measured in order to obtain the evolution in base displacement (butt curl) with time. The data acquisition rate was 1 Hz.

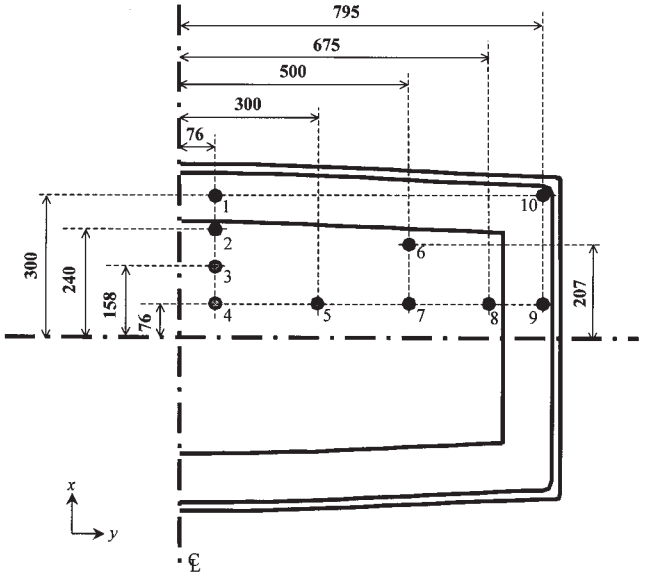

Fig. 10—Schematic of the arrangement of two thermocouple sets: one along the ingot base and the other along the top face of the bottom block (cross-sectional view).

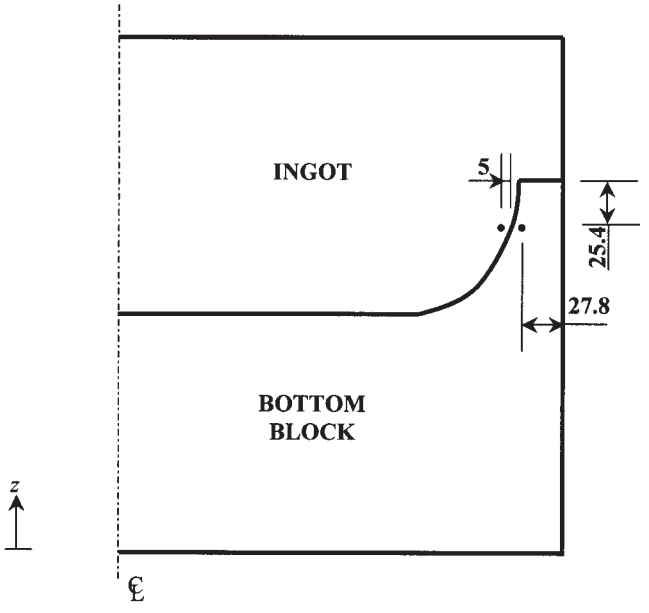

Fig. 11—Position of thermocouple placed at locations 1, 9, and 10 (refer to Fig. 10) near the ingot lip. Note: Units are in millimeters.

All of the casting parameters, including mold-fill rate, mold-fill height at the start of the cast, evolution in mold-fill height, casting withdrawal rate, and water flow rate were recorded for each cast. It should be noted that the hot casting was terminated at ~350 seconds for safety reasons, *i.e.*, to prevent the possibility of a breakout, since the temperature of the ingot would be considerably higher than what is normally observed during production.

V. RESULTS AND DISCUSSION

A. *Experimental Observations*

Figure 12 contains plots showing the variation in ingot-surface temperature with time obtained from the thermocouples located adjacent to the rolling face 10 mm above the lip, for the cold cast (casting 1) and for the hot cast (casting 2). Note that the time at which the hot cast was terminated has been identified on the plot and that the thermocouple data beyond this point should be ignored.

The thermocouple responses for both the casts indicate an initial sharp drop in temperature, from 660 °C to ~520 °C, due to meniscus cooling, followed by a rebound after ~120 seconds owing to the decrease in the rate of heat transfer after the gap formation within the mold. It is evident from a comparison of the two plots that the recipe used for casting 2 clearly yielded a "hotter" ingot, as indicated by the fact that little or no drop in temperature was observed at the point of water contact (indicated on the figure), as was observed in casting 1 (approximately 450 °C).

The substantial difference in heat transfer observed in these two cases is due to the process of water ejection caused by the presence of stable film boiling in casting 2. This phenomenon could be observed on the surface of the ingot and was indicated by a parabola-shaped line demarking the nucleate boiling regime and the ejection regime, similar to Figure 13. Within this region the ingot surface appeared dry.

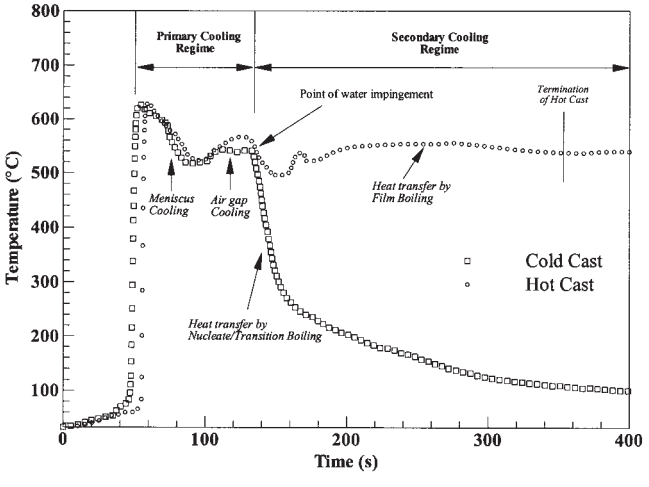

Fig. 12—Ingot subsurface temperature profiles adjacent to the rolling face and 10 mm above the ingot lip for the cold and hot casts, illustrating the different secondary cooling rates experienced by the ingot for the two different start-up conditions.

The thermocouple responses obtained from the ingot base for the two casts are also dramatically different, as can easily be seen in Figure 14, which compares the responses of the thermocouple placed near the center of the narrow face at location 9 (refer to Figure 10) for the two castings. In Figure 14, the sharp drop in the temperature observed in the cold cast at ~140 seconds (*i.e.*, a few seconds after the chill water contacted the vertical ingot faces) can be attributed to the intensive cooling caused by water entering the air gap between the ingot base and bottom block due to butt curl. This effect is not observed in the hot cast, which remained hotter for the entire casting period. This coupling between the base deflection and heat transfer clearly indicates the need to fully couple the thermal/stress analysis.

Plots showing a comparison of the evolution in ingot-base displacement for the two castings are presented in Figure 15. As can be seen, the colder casting, casting 1, resulted in a substantial increase in the base deflection in comparison to the hot casting, casting 2.

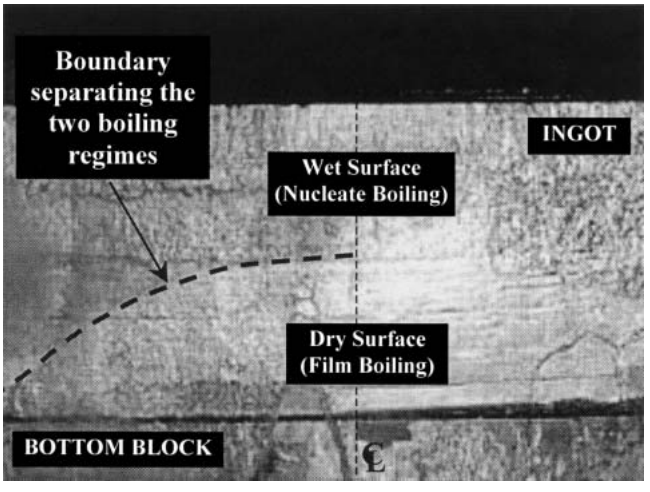

Fig. 13—The phenomenon of film boiling on the ingot surface, which was observed for the hot cast during the industrial trials. The parabola-shaped boundary, which separates the film and nucleate boiling regimes, collapsed toward the centerline as the casting progressed.

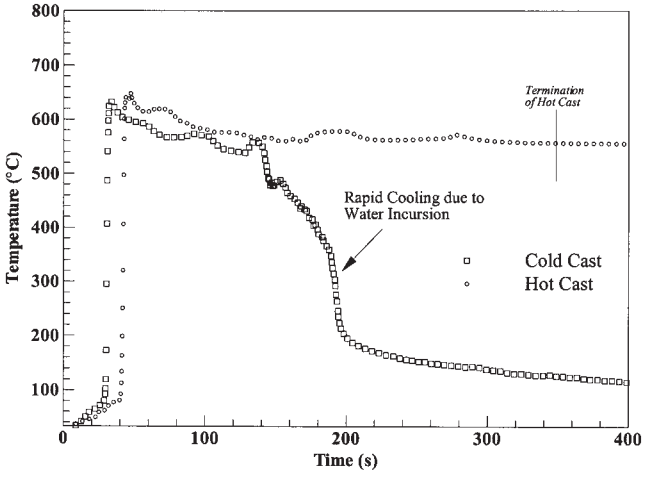

Fig. 14—Comparison between the responses of the thermocouple placed at location 9 (refer to Fig. 10) near the ingot base for the two castings.

B. *Model Predictions and Validation*

1. *Ingot sides*

The results showing a comparison between the model predictions and the measurements for the cold cast adjacent to the rolling and narrow faces are presented in Figures 16(a) and (b), respectively. The plots show the thermal history at positions 10, 60, 110, and 160 mm above the ingot lip at a location 5 mm below the surface of the face (*Note: the thermocouples located at 110 mm on the rolling face and 160 mm on the narrow face failed*). The model predictions appearing in Figure 16(b) have been corrected for the effect of butt curl, which displaced the thermocouples upward during the casting, making a direct comparison to any one node in the model incorrect. The correction was done as follows. First, using the casting recipe and butt-curl measurement data, the vertical position of the thermocouple accounting for the effect of butt curl was computed. Temperature predictions were obtained from all the nodes at or below this position. Snapshots were then extracted from these data using the appropriate nodes for the appropriate period to obtain the final "predicted curve."

Referring to Figure 16(a), it is evident that the agreement between the model predictions and the measurements is satisfactory at the various locations examined on the rolling face, apart from the tendency to underpredict the temperature near the end of the casting process at the 110 mm location. The agreement on the narrow face is somewhat poorer, particularly for the thermocouples located further from the lip. This discrepancy is likely due in part to the inability to completely correct for butt curl, using the procedure described previously.

The results showing the model predictions for the hot cast at various positions adjacent to the ingot rolling and narrow face are presented in Figures 17(a) and (b), respectively. The thermocouple data obtained at the same locations have also been plotted for comparison. *Note: the thermocouple data beyond the termination of the hot cast should be ignored.* The model was run beyond the termination of the casting to facilitate comparison to the results for the cold cast. The effect of using a lower water flow rate in the casting recipe is captured by the model that included water ejection on the ingot faces. The drop in the temperature predicted by the model at between ~350 and 420 seconds

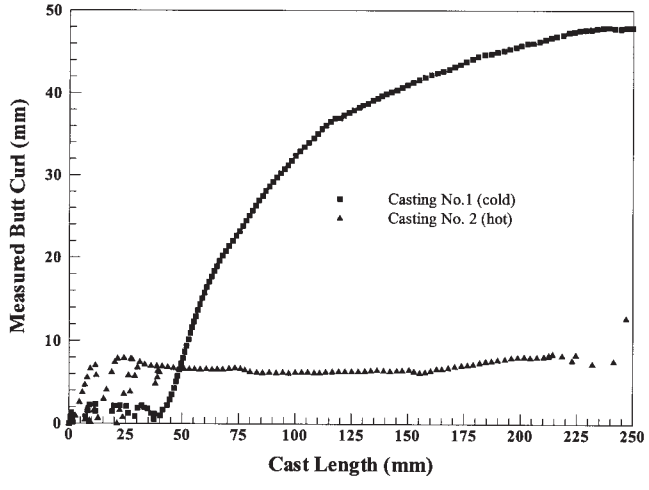

Fig. 15—Evolution of ingot base displacement (butt curl) at the center of the narrow face for the two castings.

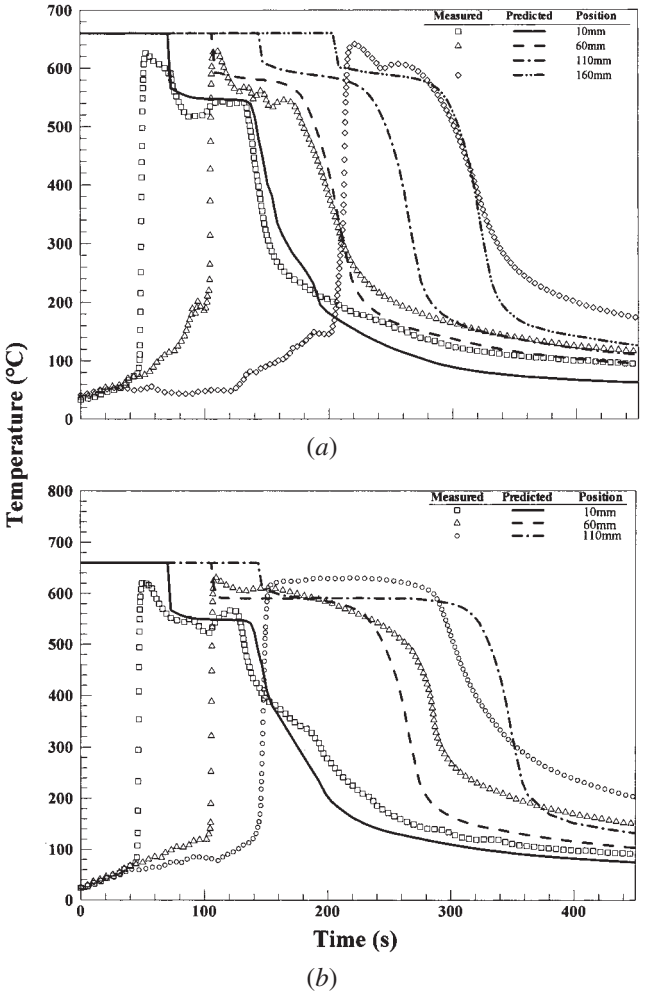

Fig. 16—Comparison of measured and model predicted temperatures at different heights (mm) above the ingot lip (refer to Fig. 9) near the center of (*a*) rolling face and (*b*) narrow face for the cold cast.

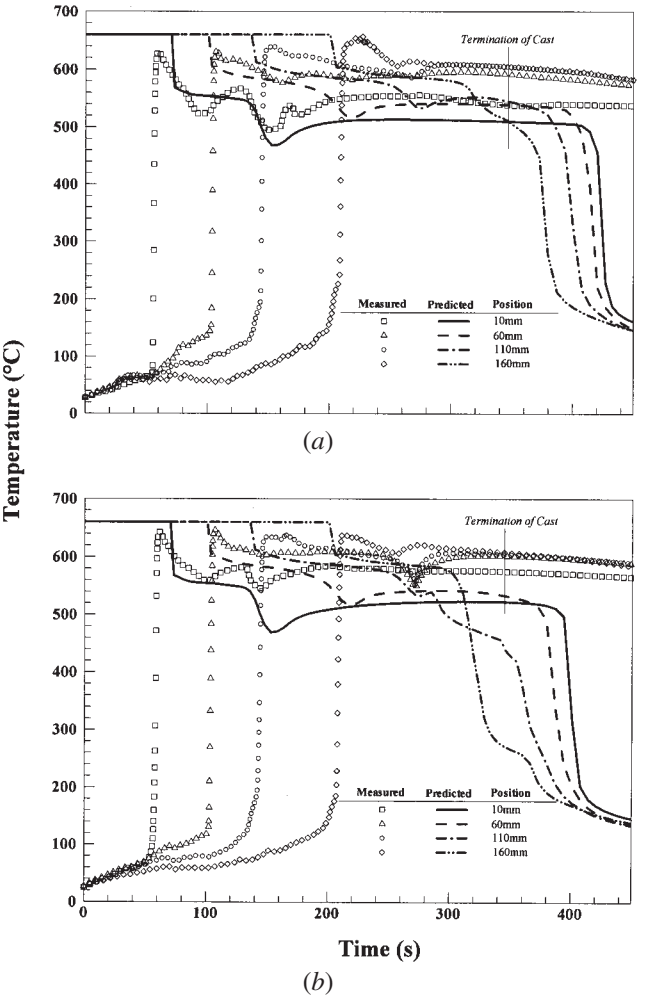

Fig. 17—Comparison of measured and model predicted temperatures at different heights (mm) above the ingot lip (refer to Fig. 9), near the center of (*a*) rolling face and (*b*) narrow face for the hot cast.

on the rolling face and between ~300 and 400 seconds on the narrow face is due to the collapse of the water-ejection front. This "collapse" is normally observed in industrial practice and is generally seen to start at the cooler corners of the casting and move toward the center and down the ingot face. It was not observed in the thermocouple data in this case, because of the early termination of the casting and the associated reduction in water flow rates. The collapse of the ejection front is observed in the model predictions, as shown by the sequential drop in the nodal temperatures starting first with the highest node located at 160 mm and ending with the lowest node located at 10 mm—refer to Figures 17(a) and (b).

Figures 18 and 19 show contour plots of temperature on the rolling and narrow faces of the ingot for the cold cast after 250 and 450 seconds, respectively. As can be seen from Figure 18, there is a small region near the center of the rolling face where film boiling prevails during the early period of the start-up phase. The ejection front quickly collapses and the ingot faces are cooled aggressively in the absence of any further film-boiling phenomenon. Figures 20 and 21 show contour plots of temperature on the rolling and narrow faces of the ingot for the hot cast after 350 and 450 seconds, respectively. The extent to which the cooling is dominated by the presence of a stable ejection front, stemming from the reduced water flow rates, is evident in the hot cast. The shape of the water-ejection front predicted by the model is strikingly similar to that observed during the industrial trials, shown in Figure 13, which demonstrates the basic validity of the ejection algorithm. It is important to realize that the presence of ejection on the ingot face represents a step change (reduction) in the heat transfer occurring at the front boundary, since, within the "ejection regime," most if not all of the water is physically removed from the surface of the ingot at positions below the point of ejection. In other words, the rate of heat transfer within this region is much lower than would be expected based on the nominal process water flow rate and surface temperatures present on the ingot surface within this region.

2. *Ingot base*

The variations in temperature with time predicted by the model 5 mm above the base of the ingot for the cold cast at various locations along lines perpendicular to the rolling face and

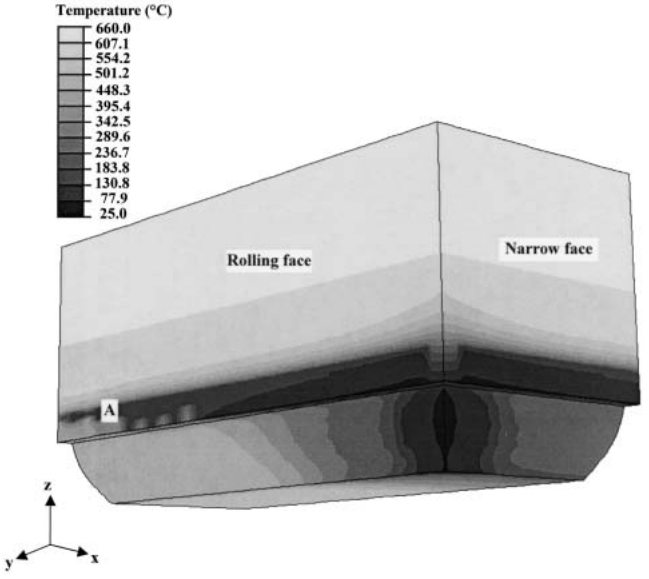

Fig. 18—Outer view of the computational domain showing the contour plot of temperature (NT11) along the rolling and narrow faces of the ingot for the cold cast after 250 s. A small area (region "A") of film boiling is predicted near the center of the rolling face. Nucleate boiling prevails in the other areas cooled by chill water.

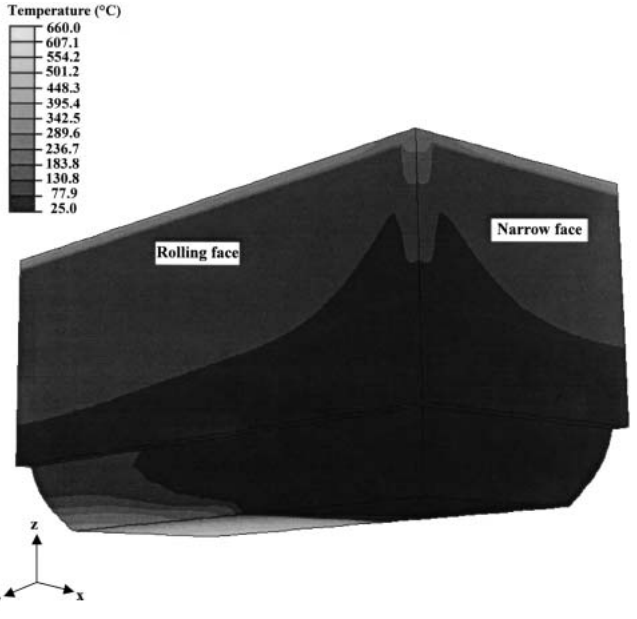

Fig. 19—Outer view of the computational domain showing the contour plot of temperature (NT11) along the rolling and narrow faces of the ingot for the cold cast at the end of the analysis, *i.e.*, after 450 s. Both the faces of ingot cooled aggressively by nucleate boiling.

perpendicular to the narrow face are presented in Figures 22(a) and (b), respectively (refer to Figure 10 for thermocouple positions). The thermocouple data obtained at the same locations have also been plotted for comparison. It is evident from the level of overall agreement that the model is able to capture most of the various heat-transfer phenomena occurring on the base of the ingot satisfactorily. The model's ability to capture the effect of water incursion is good for the thermocouples located along the line perpendicular to the narrow face

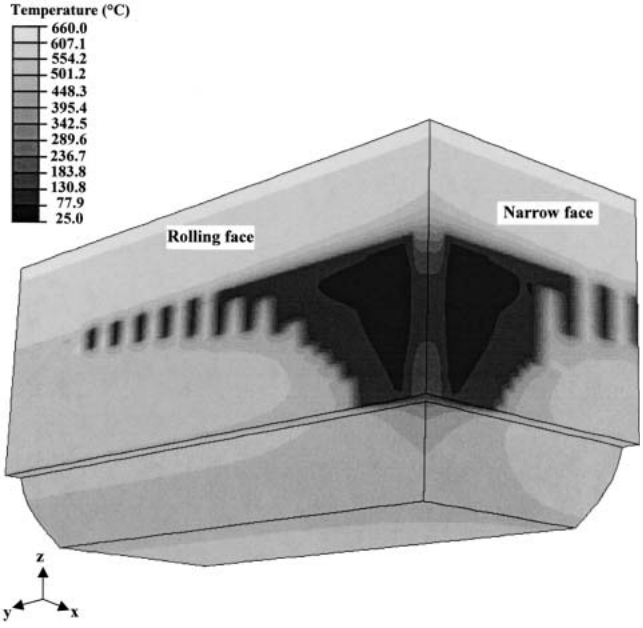

Fig. 20—Outer view of the computational domain showing the contour plot of temperature (NT11) along the rolling and narrow faces of the ingot for the hot cast at 350 s. The parabola-shaped water ejection front (or dome) separating the film and nucleate boiling regimes is clearly visible on both the surfaces.

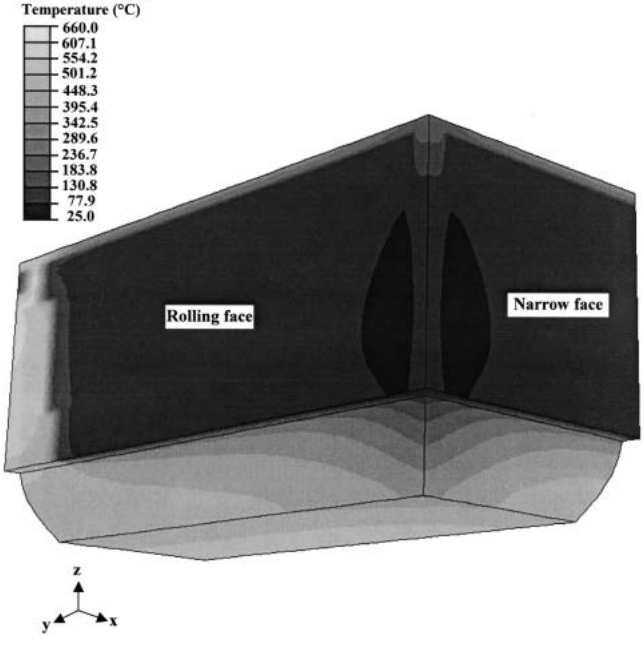

Fig. 21—Outer view of the computational domain showing the contour plot of temperature (NT11) along the rolling and narrow faces of the ingot for the hot cast at the end of the analysis, *i.e.*, after 450 s. The parabola-shaped water ejection front (or dome) separating the film and nucleate boiling regimes collapses toward the centerline on both the surfaces.

(water incursion is demarked in the thermocouple data by the rapid drop in temperature at between ~135 and ~225 seconds at locations 7 through 9 in Figure 22(b)). The trend for the locations perpendicular to the rolling face (Figure 22(a)) is not as good, with the model tending to underpredict the effect

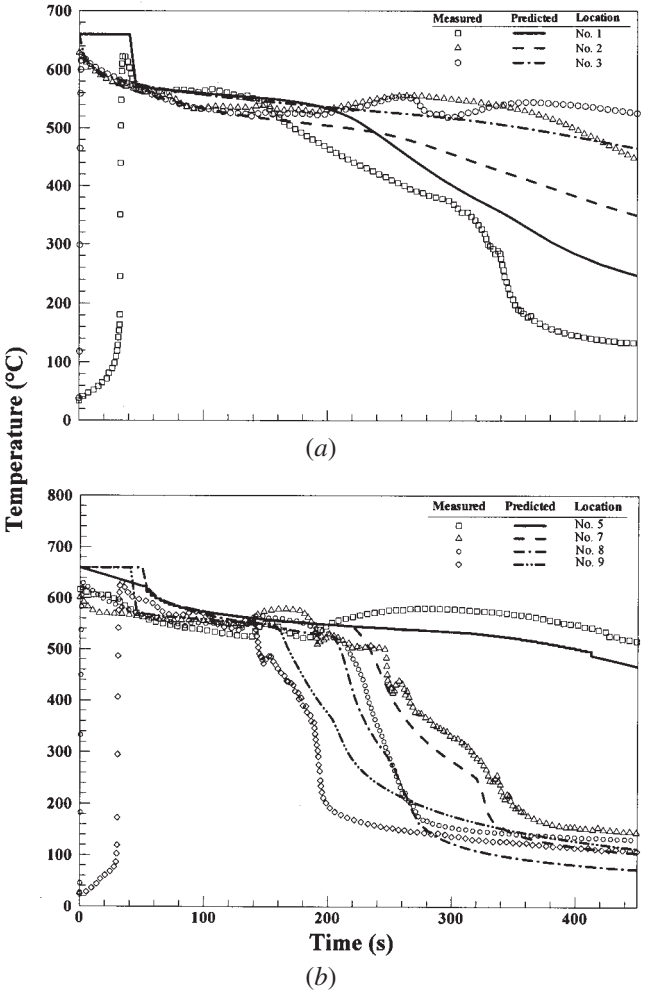

Fig. 22—Comparison of measured and model predicted temperatures at different locations 5 mm above the ingot base (refer to Fig. 10), perpendicular to the (*a*) rolling face and (*b*) narrow face for the cold cast.

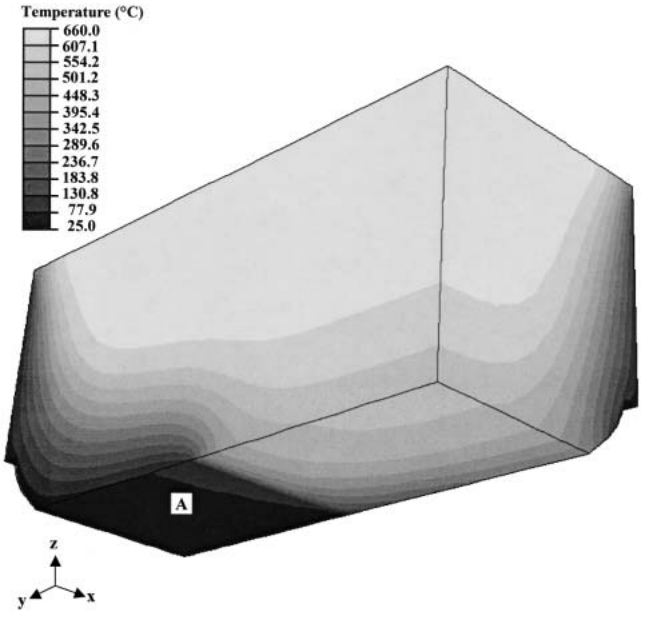

Fig. 23—Inner view of the computational domain showing the contour plot of temperature (NT11) along the symmetry faces of the ingot for the cold cast at the end of the analysis. Region "A" (area in dark gray) indicates the extent of ingot base cooling due to water incursion along the narrow face.

of the incursion at location 1 and to overpredict the effect at location 2. This problem highlights the drawback in assuming a parabolic variation in the gap profile and emphasizes the need to fully couple the thermal and stress models.

An overall view of the effect of water incursion on ingot-base cooling for the cold cast is presented in Figure 23, which shows a contour plot of temperature at the end of the analysis on the base and symmetry planes of the ingot. The plot clearly illustrates the zone on the ingot base extending from the narrow face toward the center that has been cooled by the water entrained in the gap, which has developed as a result of base deformation (indicated by dark-gray regions).

The variation in temperature with time predicted by the model in the vicinity of the base of the ingot for the hot cast is presented in Figures 24(a) and (b) together with the thermocouple data (refer to Figure 10 for thermocouple positions). It is evident from the level of overall agreement that the model is able to capture most of the various heat-transfer phenomena occurring on the base of the ingot for the hot cast satisfactorily. There is a slight trend to overpredict the cooling at locations 1 through 3, whereas the results for locations 5 through 9 are in good agreement. Overall, the results show no evidence of water incursion resulting in an ingot base that is significantly hotter than in the cold cast, by in excess of 400 °C at some locations. Contour plots of temperature on the base surface (not shown) support the conclusion drawn from the discrete thermocouple data that (1) there is no evidence of water incursion and (2) the ingot base is significantly hotter in certain regions.

3. *Bottom block*

The variation in temperature with time predicted by the model 5 mm below the top face of the bottom block for the cold cast is presented in Figures 25(a) and (b) together with the thermocouple data. As in the case of the ingot-base thermocouples, there is clear evidence of water incursion (location 1, Figure 25(a) and Locations 7 through 9, Figure 25(b)), which is indicated by the rapid drop in temperature. The model is able to capture this behavior satisfactorily overall; however, the agreement is better for those thermocouple positions located adjacent to the narrow face than for those located adjacent to the to the broad face. This variation in the predictive capability is consistent with the results obtained for the ingot base and reflects the limitations in the assumption of a parabolic deformation of the base.

A contour plot showing the extent of the water-incursion cooling on the top of the bottom block predicted by the model is presented in Figure 26. It is evident that the cooling extends from the narrow side in toward the center of the casting. There is also some cooling by water evident in the predictions adjacent to the rolling face and on the upper portion of the lip.

The predictions for the bottom block for the hot cast are presented in Figures 27(a) and (b), together with thermocouple data at the appropriate locations. As can be seen, the model accurately predicts the overall trends in the thermocouple satisfactorily. Focusing on thermocouples at locations 1 and 9, it is interesting to note that the model initially predicts a rapid heat up in these regions, which is followed by

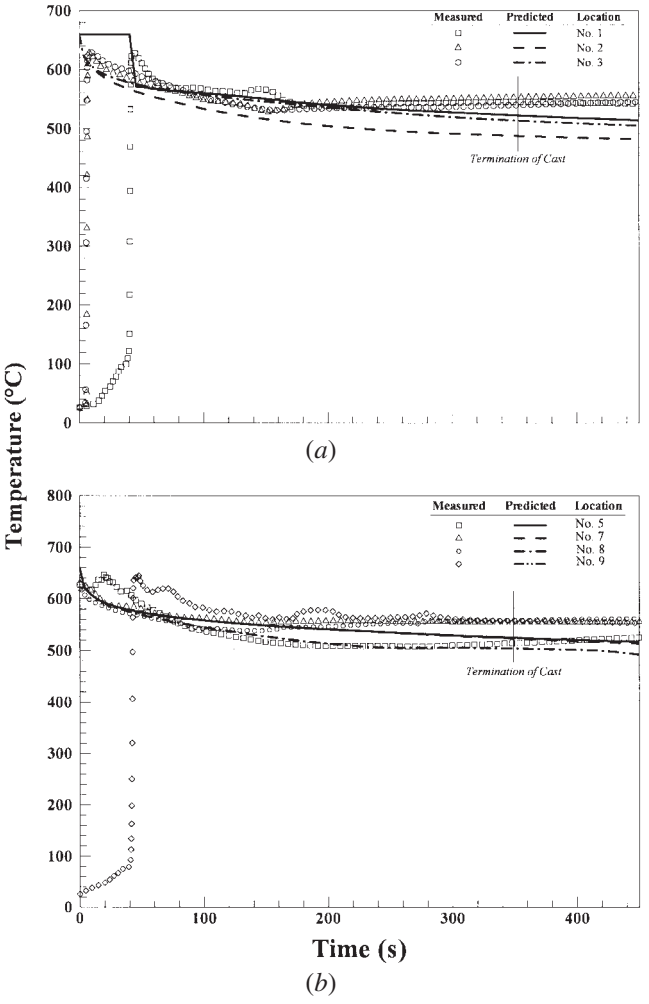

Fig. 24—Comparison of measured and model predicted temperatures at different locations 5 mm above the ingot base (refer to Fig. 10), perpendicular to the (*a*) rolling face and (*b*) narrow face for the hot cast.

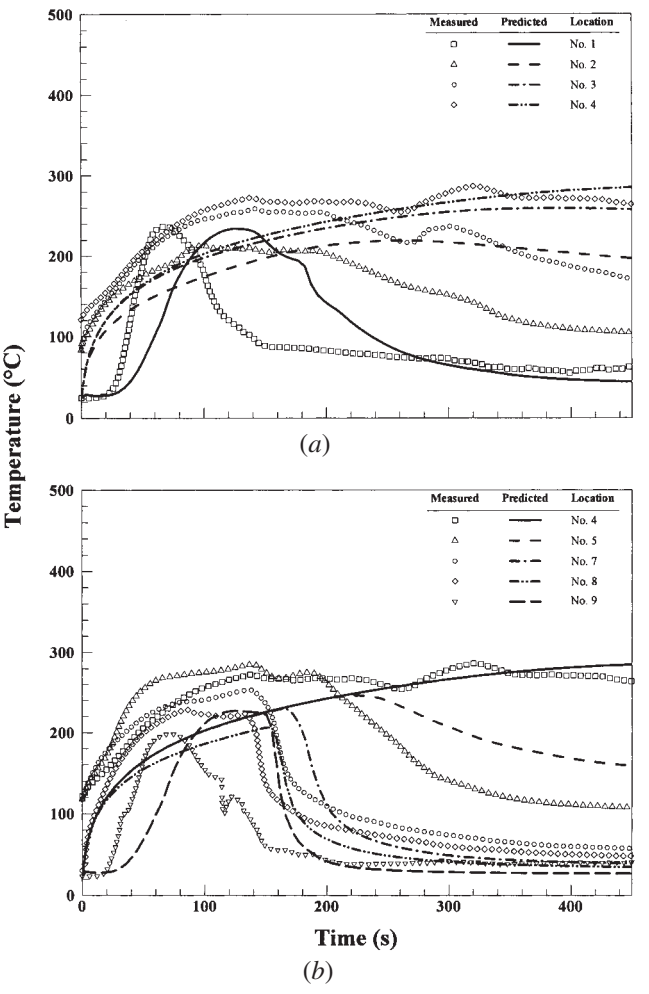

Fig. 25—Comparison of measured and model predicted temperatures at different locations 5 mm below the bottom block top face (refer to Fig. 10), perpendicular to the (*a*) rolling face and (*b*) narrow face for the cold cast.

a short term drop and then a second increase in temperature. The initial drop in temperature arises due to the water flowing down the vertical edges of the removal of bottom block and water incursion into the gap. The subsequent rise in temperature occurs as a result of the removal of water from the surface of the bottom block associated with ejection occurring further up the face of the ingot.

C. *Implications for Process Control*

The experimental program outlined previously and the associated mathematical analysis with a comprehensive heat-transfer model has identified a number of interrelated heat-transfer phenomena occurring during the start-up phase. From a process-control standpoint, both water incursion and water ejection are problematic, as the combination leads to extremes in cooling conditions. For example, low water flow rates that lead to water ejection result in a substantial reduction (step change) in heat transfer within specific regions of the ingot face experiencing this behavior. This reduction in heat transfer on the sides of the ingot limits ingot-base displacement and suppresses water incursion, which, in turn, leads to a substantial reduction in heat transfer on the base of the ingot. Thus, two of the three major heat-transfer mechanisms (secondary and base cooling) are substantially reduced during the start-up phase for hot casts. Conversely, relatively high water flow rates that suppress water ejection lead to butt curl, water incursion, and high rates of heat transfer from specific areas on the base of the ingot. Thus, secondary and base cooling are substantially enhanced during the start-up phase. The transition from these two extremes in behavior is obviously critical from the standpoint of process control.

VI. SUMMARY AND CONCLUSIONS

A comprehensive mathematical model has been developed to describe heat transfer during the start-up phase of the DC casting process. The model includes primary cooling by the mold, secondary cooling by water, and ingot-base cooling. The algorithm used to account for secondary cooling by the water includes boiling curves that are a function of surface temperature, impingement-point temperature, water flow rate, and position relative to the point of water impingement. In addition, the secondary-cooling algorithm includes

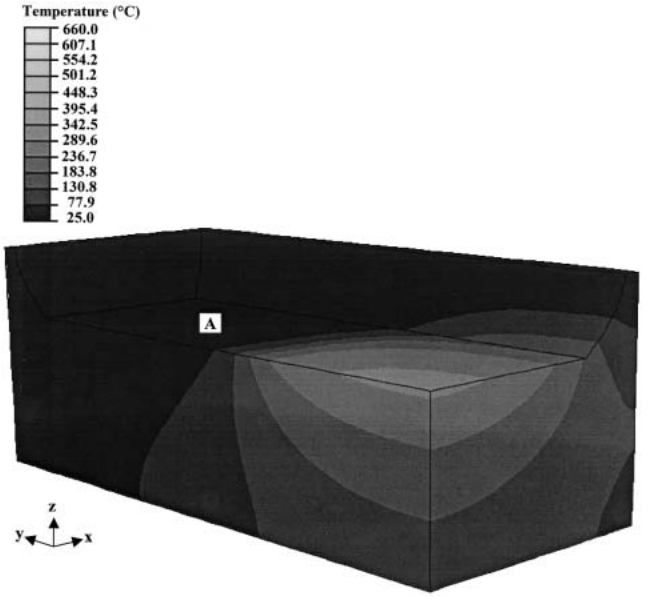

Fig. 26—Inner view of the computational domain showing the contour plot of temperature (NT11) along the symmetry faces of the bottom block for the cold cast at the end of the analysis. Region "A" (area in dark gray) indicates the extent of bottom block cooling due to water incursion along the rolling and narrow faces.

water ejection, which can occur at low water flow rates (low heat-extraction rates). The algorithm used to describe ingot-base cooling includes the drop in contact heat transfer due to base deformation (butt curl) and also the increase in heat transfer due to water incursion between the ingot base and the bottom block.

Temperature measurements obtained at various locations on the ingot surface adjacent to the rolling face and adjacent to the ingot base clearly show the effect of both water ejection and water incursion. The effect of water incursion can also be seen in data collected from the bottom block adjacent to the top surface.

The temperatures predicted by the 3-D model show satisfactory overall agreement with the measured temperature data for both the cold and hot casts, which were distinguished by the different start-up cooling conditions experienced by the ingot. Once established through trial-and-error fitting, a common set of tunable parameters used in characterization of the boundary conditions have been used to describe both extremes in casting behavior. The model adequately captured start-up conditions that triggered film boiling and water ejection on the ingot surfaces and their subsequent effect on the secondary-cooling heat transfer, including the collapse of the parabola-shaped water-ejection front, which was observed during the hot cast. The model also satisfactorily captured the influence of butt curl and entrained water on ingot-base cooling during the start-up phase.

The distinctly different spatial variations in temperature of the bottom block predicted by the model for the cold and hot casts indicated that the bottom block played a significant role in dictating the heat transfer from the base of the ingot during the start-up phase. The thermal behavior of the bottom block was clearly influenced by the evolution of the butt curl and the process of water incursion.

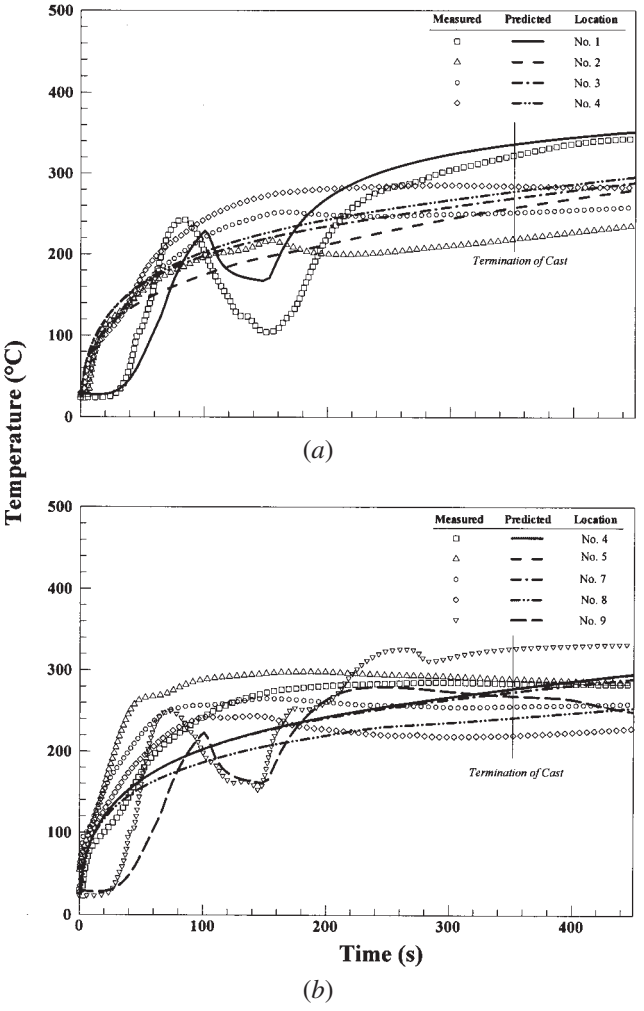

Fig. 27—Comparison of measured and model predicted temperatures at different locations 5 mm below the bottom block top face (refer to Fig. 10), perpendicular to the (*a*) rolling face and (*b*) narrow face for the hot cast.

In its current form, the uncoupled analysis is limited by the need for measured data for the evolution of butt curl at the center of the rolling and narrow faces of the ingot.

ACKNOWLEDGMENTS

The authors are grateful to the Natural Sciences and Engineering Research Council of Canada for providing financial support and to Alcan International's Arvida Research and Development Centre for providing financial support and expertise.

NOMENCLATURE

$c_p(T)$	specific heat capacity as a function of temperature, T	J kg^{-1} K^{-1}
f	a polynomial function	—
f_s	volume fraction solidified	—
f_{wet}	wetting factor for water incursion	—
h	convective heat-transfer coefficient	W m^{-2} K^{-1}
h_{airgap}	heat-transfer coefficient associated with air gap	W m^{-2} K^{-1}

$h_{contact}$	heat-transfer coefficient associated with meniscus	W m^{-2} K^{-1}
h_{gap}	gap conductance coefficient at the ingot/bottom block interface	W m^{-2} K^{-1}
h_{water}	boiling water heat-transfer coefficient	W m^{-2} K^{-1}
i,j,k	counters in an algorithm	—
k	thermal conductivity	—
$k(T)$	thermal conductivity as a function of temperature, T	W m^{-1} K^{-1}
L	latent heat of fusion	J kg^{-1}
n	direction cosine normal to the ingot surface	—
q	heat flow rate per unit area	W m^{-2}
Q	water flow rate per unit length of mold perimeter	L min^{-1} cm^{-1}
$\dot{Q}$	volumetric heat source term	W m^{-3}
t	time	s
T	temperature	°C
T_o	initial temperature	°C
$T_{bottomblock}$	temperature of the bottom block	°C
T_{ingot}	temperature of the ingot	°C
T_L	liquidus temperature of AA5182	°C
T_S	solidus temperature of AA5182	°C
T_{Sink}	sink temperature	°C
T_{Surf}	ingot surface temperature	°C
x	direction along the narrow face of the ingot in the Cartesian coordinate system	—
X_1	half-thickness of the ingot	m
X_2	extent of water incursion in the ingot along x direction	m
X_3	extent of water incursion in the bottom block along x direction	m
y	direction along the rolling face of the ingot in the Cartesian coordinate system	—
Y_1	half-width of the ingot	m
Y_2	extent of water incursion in the ingot along y direction	m
Y_3	extent of water incursion in the bottom block along y direction	m
z	direction along the cast length in the Cartesian coordinate system	—
z'	distance from the water impingement point	m
z_{max}	maximum butt curl measured at ingot corner	m
Greek Symbols		
Γ	surface enclosing the computational domain	—
ρ	density	kg m^{-3}
Ω	computational domain	—
∂	partial derivative operator	—

REFERENCES

1. J.-M. Drezet: Ph.D. Thesis, Ecole Polytechnique Federale de Lausanne, Lausanne, Switzerland, 1996.
2. J.B. Wiskel: Ph.D. Thesis, University of British Columbia, Vancouver, 1996.
3. J.F. Grandfield and P.T. McGlade: *Mater. Forum*, 1996, vol. 20, pp. 29-51.
4. J.E. Jacoby: *Proc. 5th Australasian Asian Pacific Conf. on Aluminum Cast House Technology*, M. Nilmani, P. Whiteley, and J. Grandfield, eds., TMS, Warrendale, PA, 1997, pp. 245-51.
5. W. Droste and W. Schneider: in *Light Metals 1991*, E.L. Rooy, ed., TMS, Warrendale, PA, 1991, pp. 945-51.
6. H.G. Fjaer and A. Mo: in *Light Metals 1995*, J. Evans, ed., TMS, Warrendale, PA, 1995, pp. 951-59.
7. Y. Caron and A. Larouche: in *Light Metals 1996*, W. Hale, ed., TMS, Warrendale, PA, 1996, pp. 963-69.
8. H. Yu: in *Light Metals 1980*, TMS, Warrendale, PA, 1980, pp. 613-28.
9. Wagstaff, Inc.: U.S. Patent 4, 693, 298, 1987.
10. N.B. Bryson: U.S. Patent 3, 411, 079, 1969.
11. W. Schneider and E.K. Jensen: in *Light Metals 1990*, C.M. Bickert, ed., TMS, Warrendale, PA, 1990, pp. 931-36.
12. W. Schneider, E.K. Jensen, and B. Carrupt: in *Light Metals 1995*, J. Evans, ed., TMS, Warrendale, PA, 1995, pp. 961-67.
13. H.G. Fjaer and A. Mo: *Metall. Trans. B*, 1990, vol. 21B, pp. 1049-61.
14. E.K. Jensen and W. Schneider: in *Light Metals 1990*, C.M. Bickert, ed., TMS, Warrendale, PA, 1990, pp. 937-43.
15. H.G. Fjaer and E.K. Jensen: in *Light Metals 1995*, J. Evans, ed., TMS, Warrendale, PA, 1995, pp. 951-59.
16. E.K. Jensen and W. Schneider: in *Light Metals 1995*, J. Evans, ed., TMS, Warrendale, PA, 1995, pp. 969-78.
17. B. Hannart, F. Cialti, and R.V. Schalkwijk: in *Light Metals 1994*, U. Mannweiler, ed., TMS, Warrendale, PA, 1994, pp. 879-87.
18. J.-M. Drezet and M. Rappaz: *Metall. Mater. Trans. A*, 1996, vol. 27A, pp. 3214-24.
19. J.B. Wiskel and S.L. Cockcroft: *Metall. Mater. Trans. B*, 1996, vol. 27B, pp. 119-27.
20. J.B. Wiskel and S.L. Cockcroft: *Metall. Mater. Trans. B*, 1996, vol. 27B, pp. 29-137.
21. J. Du, B.S.-J. Kang, K.-M. Chang, and J. Harris: in *Light Metals 1998*, B. Welch, ed., TMS, Warrendale, PA, 1998, pp. 1025-29.
22. H.G. Fjaer, D. Mortensen, A. Hakonsen, and E. Sorheim: in *Light Metals 1999*, C.E. Eckert, ed., TMS, Warrendale, PA, 1999, pp. 743-48.
23. W. Droste, J.-M. Drezet, G.-U. Grun, and W. Schneider: in *Continuous Casting*, K. Ehrke and W. Schneider, eds., Wiley-VCH, New York, NY, 2000, pp. 177-83.
24. J. Sengupta, D. Maijer, M.A. Wells, and S.L. Cockcroft: *Proc. Brimacombe Memorial Symp*., Canadian Institute of Mining, Metallurgy and Petroleum, Montreal, Canada, 2000, pp. 673-684.
25. J. Sengupta, D. Maijer, M.A. Wells, S.L. Cockcroft, and A. Larouche: in *Light Metals 2001*, J.L. Anjier, ed., TMS, Warrendale, PA, 2001, pp. 879-85.
26. J. Sengupta, S.L. Cockcroft, D. Maijer, M.A. Wells, and A. Larouche: *J. Light Met*., 2002, No. 2, pp. 137-48.
27. D.C. Weckman and P. Niessen: *Metall. Trans. B*, 1982, vol. 13B, pp. 593-602.
28. W. Schneider and W. Reif: *Proc. 6th Arab Int. Aluminum Conf. (ARABAL '93)*, Arab Federation for Engineering Industries, Cairo, Egypt, 1994, pp. 173-90.
29. K. Ho and R.D. Pehlke: *Metall. Trans. B*, 1985, vol. 16B, pp. 585-94.
30. Y. Nishida, W. Droste, and E. Engler: *Metall. Trans. B*, 1986, vol. 17B, pp. 833-44.
31. M. Trovant and S. Argyropoulos: in *Light Metals 1997*, R. Huglen, ed., TMS, Warrendale, PA, 1997, pp. 927-31.
32. H.G. Fjaer and A. Hakonsen: in *Light Metals 1997*, R. Huglen, ed., TMS, Warrendale, PA, 1997, pp. 683-90.
33. H. Kraushaar, R. Jeschar, V. Heidt, E.K. Jensen, and W. Schneider: in *Light Metals 1995*, J. Evans, ed., TMS, Warrendale, PA, 1995, pp. 1055-59.
34. J. Langlais, T. Bourgeois, Y. Caron, G. Beland, and D. Bernard: in *Light Metals 1995*, J. Evans, ed., TMS, Warrendale, PA, 1995, pp. 979-86.
35. L. Maenner, B. Magnin, and Y. Caratini: in *Light Metals 1997*, R. Huglen, ed., TMS, Warrendale, PA, 1997, pp. 701-07.
36. A. Larouche, Y. Caron, and D. Kocaefe: in *Light Metals 1998*, B. Welch, ed., TMS, Warrendale, PA, 1998, pp. 1059-64.
37. A. Larouche, J. Langlais, T. Bourgeois, and A. Gendron: in *Light Metals 1999*, M. Bouchard and A. Faucher, eds., TMS, Warrendale, PA, 1999, pp. 235-45.
38. I.J. Opstelten and J.M. Rabenberg: in *Light Metals 1999*, C.E. Eckert, ed., TMS, Warrendale, PA, 1999, pp. 729-35.
39. J. Zuidema, Jr., L. Katgerman, I.J. Opstelten, and J.M. Rabenberg: in *Light Metals 2001*, J.L. Anjier, ed., TMS, Warrendale, PA, 2001, pp. 873-78.

40. D. Li, M.A. Wells, and G. Lockhart: in *Light Metals 2001*, J.L. Anjier, ed., TMS, Warrendale, PA, 2001, pp. 865-71.
41. M.A. Wells, D. Li, and S.L. Cockcroft: *Metall. Mater. Trans. B*, 2000, vol. 32B, pp. 929-39.
42. L.I. Kiss, T. Meenken, A. Charette, Y. Lefebvre, and R. Levesque: *Light Metals 2002*, W. Schneider, ed., TMS, Warrendale, PA, 2002, pp. 981-85.
43. J.A. Bakken and T. Bergstrom: in *Light Metals 1986*, TMS, Warrendale, PA, 1986, pp. 883-89.
44. E.K. Jensen, S. Johansen, Bakken, T. Bergstrom, and J.A. Bakken: in *Light Metals 1986*, TMS, Warrendale, PA, 1986, pp. 891-96.
45. Y. Watanabe and N. Hayashi: in *Light Metals 1996*, W. Halen, ed., TMS, Warrendale, PA, 1996, pp. 979-84.
46. J.-M. Drezet, G.-U. Gruen, and M. Gremaud: in *Light Metals 2000*, R.D. Peterson, ed., TMS, Warrendale, PA, 2000, pp. 585-90.
47. D.C. Weckman and P. Niessen: *Can. Metall. Q.*, 1984, vol. 23 (2), pp. 209-16.
48. J.F. Grandfield, A. Hoadley, and S. Instone: in *Light Metals 1997*, R. Huglen, ed., TMS, Warrendale, PA, 1997, pp. 691-99.
49. E.A. Sorheim, D. Mortensen, S. Benum, and C. Stette: in *Light Metals 2002*, W. Schneider, ed., TMS, Warrendale, PA, 2002, pp. 679-86.
50. E.D. Tarapore: *Light Metals 1989*, P.G. Campbell ed., TMS, Warrendale, PA, 1989, pp. 875-79.
51. G.P. Grealy, J. Lee Davis, E.K. Jensen, P.A. Tondel, and J. Moritz: in *Light Metals 2001*, J.L. Anjier, ed., TMS, Warrendale, PA, 2001, pp. 813-21.